J Mater Sci: Mater Electron (2016) 27:1974–1982
DOI 10.1007/s10854-015-3980-5

Novel size-controlled fabrication of pure $Zn_3V_2O_8$ nanostructures via a simple precipitation approach

Fatemeh Mazloom[1] · Maryam Masjedi-Arani[1] · Masoud Salavati-Niasari[1]

Received: 22 July 2015 / Accepted: 25 October 2015 / Published online: 11 November 2015

Abstract Pure zinc vanadate ($Zn_3V_2O_8$) nanostructures were prepared via a simple precipitation approach by using different amines as novel basic agents. Various amines and surfactants were applied and the as-prepared products were characterized using X-ray diffraction, scanning electron microscopy, transmission electron microscopy, Fourier transform infrared spectrum, Electron Dispersive X-ray spectroscopy, Photoluminescence and ultraviolet–visible (UV–Vis) spectroscopy. Zinc vanadate nanostructures with different particle size and morphology were prepared successfully. The photocatalytic activity of $Zn_3V_2O_8$ nanostructure was investigated by degradation of anionic dye of eosin Y in aqueous solution under UV light irradiation.

1 Introduction

In the last few decades, nanotechnology has attracted significant consideration due to its extensive applications in industry and our lives [1–3]. Metal vanadates are a significant class of inorganic nanomaterials that have received main interest as complex oxides due to their potential application in diverse fields e.g., catalysis [4], cathode materials in batteries [5], implantable cardiac defibrillators (ICDs) [6] and low-temperature magnetic devices [7]. Lots of research has been focused on the synthesis of metal vanadates of silver, copper, manganese, iron, bismuth and indium from different approaches. Among them, zinc vanadate nanomaterials have interested special attention since zinc is a cheap, abundant and environmental-benign metal, and vanadium has multiple valence states leading to rich structures of its compounds. Nanostructured $Zn_3V_2O_8$ is widely used in applications such as lithium ion batteries [8], photocatalysis [9], and luminescence [10, 11]. A variation of possible methods including hydrothermal method [12], sol–gel [13], wet chemical approach [9], coprecipitation [8] and solid state [11, 14] have been applied to obtain different types of zinc vanadate. Herein, we develop the precipitation method to synthesize of $Zn_3(VO_4)_2$ nanocrystals. The precipitation method is a suitable synthesis process for prepare of many inorganic powders. This method is simple, convenient and cost effective synthetic procedure and provides an effective way to the synthesis of uniform nanocrystals. In this method, crystallization way is performed at low temperature and design of reaction condition is very flexible. In this paper, $Zn_3V_2O_8$ nanoparticles were synthesized by a precipitation method using novel basic agents to adjust the pH value to 8–9. The purpose of this study is investigating the role of different amines on the size, morphology and uniformity of the pure $Zn_3V_2O_8$ nanocrystals. The selected amines are chosen in a way that we investigate the effect of different amines with different nitrogen active sites. The long carbon chain of amines can provide great steric hindrance to control the size of nanoparticles [15, 16]. The effects of different parameters such as various amines and surfactants on the product size, morphology and uniformity were also investigated. Moreover, the photocatalytic degradation activity of anionic dye of eosin Y as water pollutant is performed to study the catalytic properties of as-produced $Zn_3V_2O_8$ nanostructures.

✉ Masoud Salavati-Niasari
Salavati@kashanu.ac.ir

[1] Institute of Nano Science and Nano Technology, University of Kashan, Kashan, P.O. Box 87317-51167, Islamic Republic of Iran

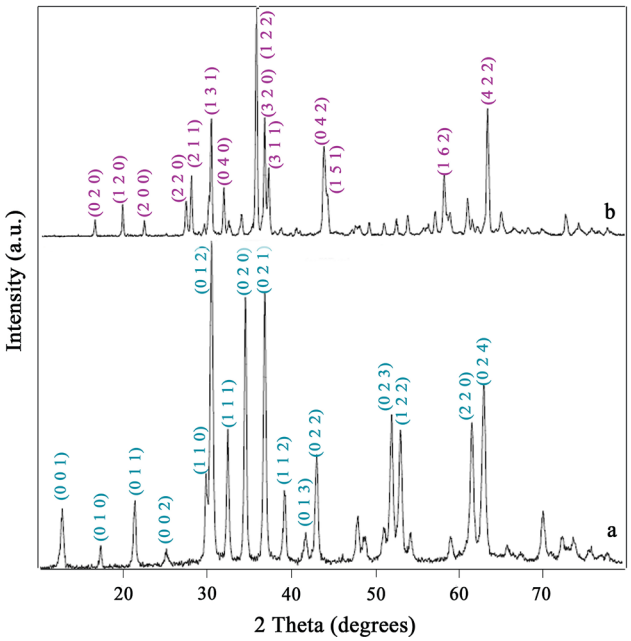

Fig. 1 XRD patterns of synthesized samples *a* before and *b* after calcination

2 Experimental

2.1 Materials and physical measurements

$Zn(NO_3)_2{\cdot}4H_2O$, NH_4VO_3, NH_3, ethylenediamine (en), propylenediamine (pn), butylenediamine (bn), triethylenetetramine (TETA), tetraethylenepentamine (TEPA) were purchased from Merck Company. All of the chemicals were used as received without further purifications. For characterization of the products, X-ray diffraction (XRD) patterns were recorded by a Rigaku D-max C III, X-ray diffractometer using Ni-filtered Cu Ka radiation. Scanning electron microscopy (SEM) images were obtained on Philips XL-30ESEM. Transmission electron microscopy (TEM) image was obtained on a Philips EM208 transmission electron microscope with an accelerating voltage of 200 kV. Fourier transform infrared (FT-IR) spectra were recorded on Shimadzu Varian 4300 spectrophotometer in KBr pellets. Optical analyses were performed using a V-670 UV–Vis–NIR Spectrophotometer (Jasco). Room temperature photoluminescence (PL) was studied on a Perkin Elmer (LS 55) fluorescence spectrophotometer. The magnetic properties of the samples were detected at room temperature using a vibrating sample magnetometer (VSM, Meghnatis Kavir Kashan Co., Kashan, Iran).

2.2 Synthesis of pure $Zn_3V_2O_8$ nanoparticles

$Zn(NO_3)_2{\cdot}4H_2O$ was dissolved into deionized water to form a transparent solution. Then NH_4VO_3 with a molar ratio of Zn:V = 3:2 was dissolved into another deionized water at 80 °C. After that, the NH_4VO_3 solution was added slowly to the Zn solution under stirring. In this process, a yellow suspension appeared gradually. Finally, basic agent was added to adjust the pH value of the solution to about 8–9, after the mixture had been stirred for about 2 h. The final products were collected by centrifugation, washed with deionized water and ethanol. The as-obtained products were dried at 80 °C under vacuum for 2 h, then calcinated at 600 °C for another 2 h.

2.3 Photocatalytic measurements

The photocatalytic activity of $Zn_3V_2O_8$ nanoparticles was tested by using eosin Y solution. The degradation reaction was carried out in a quartz photocatalytic reactor. The

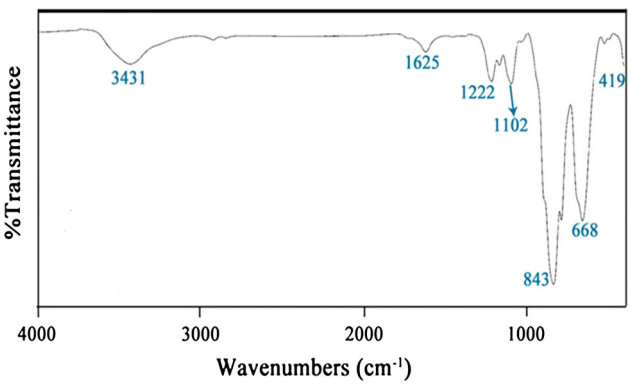

Fig. 2 FT-IR spectrum of $Zn_3V_2O_8$ nanoparticles (sample No. 9)

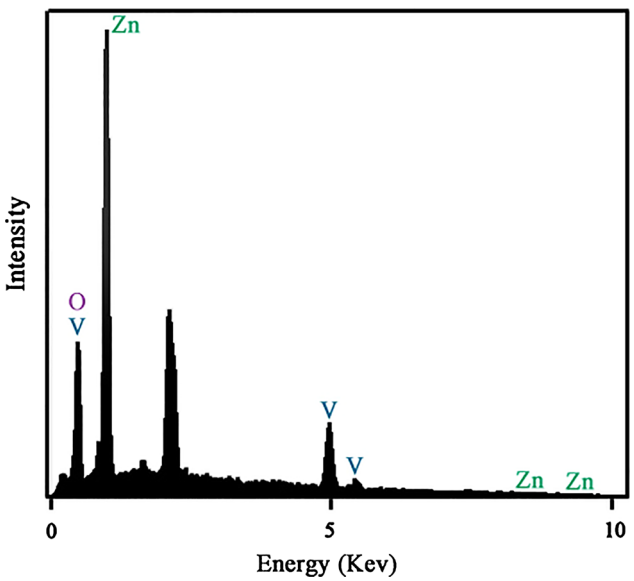

Fig. 3 EDS pattern of $Zn_3V_2O_8$ nanoparticles (sample No. 9)

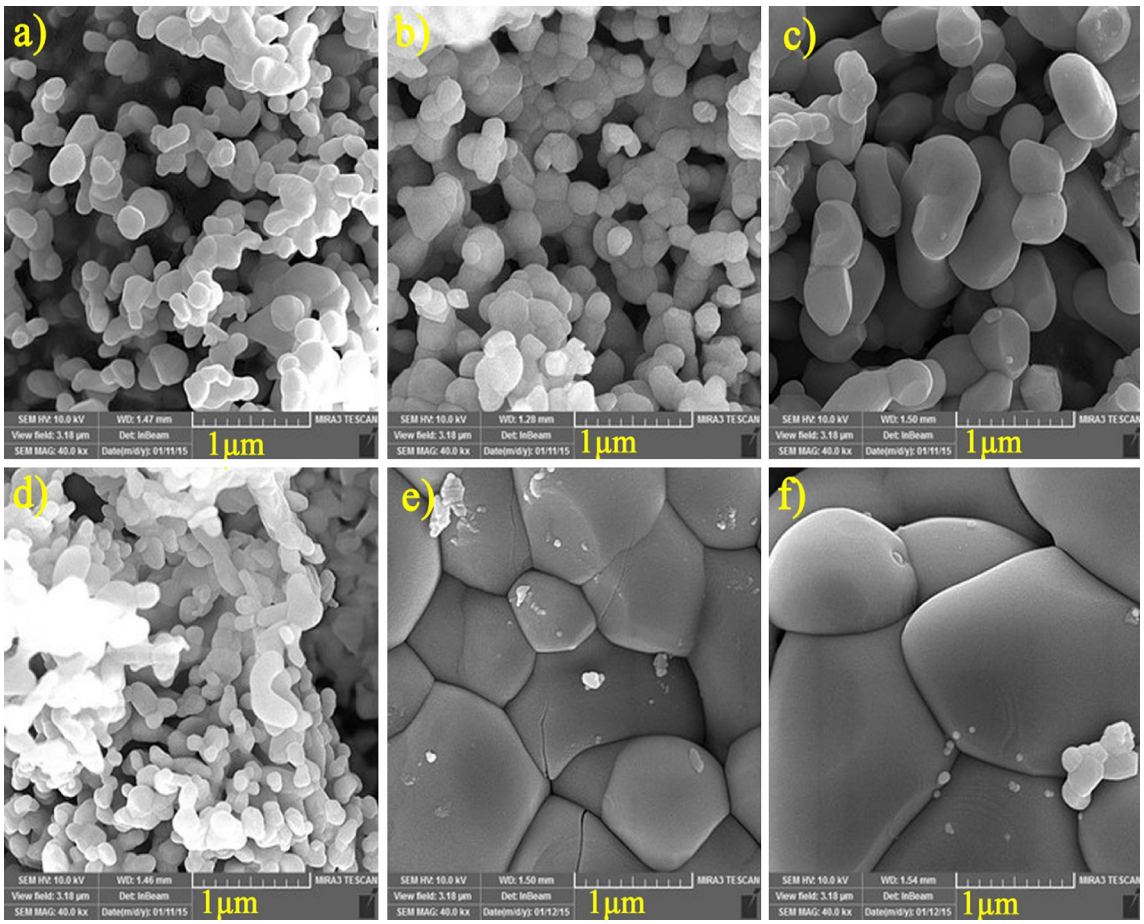

Fig. 4 SEM images of $Zn_3V_2O_8$ nanostructures prepared by different amines **a** NH_3, **b** en, **c** pn, **d** bn, **e** TETA, **f** TEPA

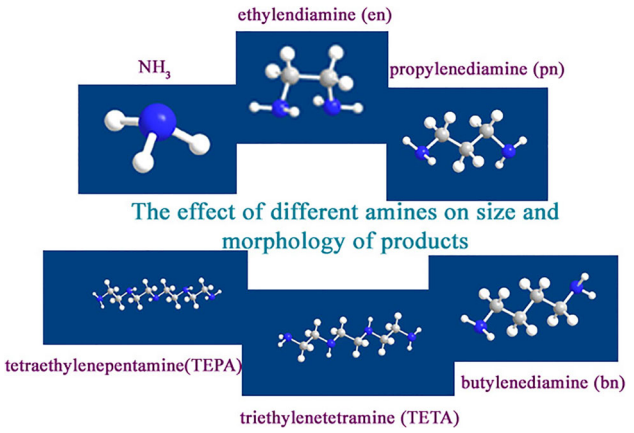

Scheme 1 Different amines used for preparation of $Zn_3V_2O_8$ nanostructures

Table 1 Reaction conditions for Zinc Vanadium Oxide nanostructures

Sample no	Type of amine	Surfactant	Particle size (SEM)
1	NH_3	–	75–190 nm
2	en	–	28–400 nm
3	pn	–	300–450 nm
4	bn	–	40–270 nm
5	TETA	–	0.5–1 µm
6	TEPA	–	0.5–2 µm
7[a]	–	–	0.5–1 µm
8	en	CTAB	1–2.5 µm
9	en	SDS	35–120 nm
10	en	PVP	45–250 nm

[a] Blank test

photocatalytic degradation was carried out with 5×10^{-5} M of eosin Y solution containing 0.05 g of nanostructures. This mixture was aerated for 30 min to reach adsorption equilibrium. Then, the mixture was placed inside the photoreactor in which the vessel was 40 cm away from the UV. The quartz vessel and light sources were placed inside a black box equipped with a fan to prevent UV leakage. The experiments were performed at room temperature and pH of the eosin Y solution was adjusted 3. Aliquots of the mixture were taken at periodic intervals during the irradiation, and after centrifugation they were analyzed with the UV–Vis

spectrometer. The dyes degradation percentage was calculated as follows:

$$D.P.(t) = \frac{A0 - At}{A0} \times 100 \quad (1)$$

Where A_0 and A_t are the absorbance value of solution at 0 and t min, respectively.

3 Results and discussion

3.1 X-ray diffraction patterns

The X-ray diffraction patterns of as-prepared products obtained from the precipitation route are shown in Fig. 1. Figure 1a, b show the XRD patterns of Zinc Vanadium Oxide samples before and after calcinations, respectively. Most of the reflection peaks in Fig. 1a can be assigned to hexagonal phase $Zn_3V_2O_7(OH)_2{\cdot}2H_2O$ (JCPDS 50-0570) by comparing with the standard pattern. Figure 1b shows XRD pattern of $Zn_3V_2O_8$ (JCPDS 34-0378) nanoparticles after calcination. All diffraction peaks can be well indexed to pure orthorhombic structural Zinc Vanadium Oxide with space group of Abam and cell constants a = 8.2990 Å, b = 11.5284 Å, c = 6.1116 Å. No peak from other phases has been detected, indicating the high purity of the product and the sharp reflection peaks confirmed high crystallinity of the as-prepared $Zn_3V_2O_8$. The average crystallite size of the as-synthesized product was determined from Debeys–Scherrer equation [17] given by the following equation: $D = K\lambda/\beta\cos\theta$; where β is the breadth of the observed diffraction line at its half intensity maximum, K is the so-called shape factor, which usually takes a value of about 0.9, and λ is the wavelength of X-ray source used in XRD. The average crystallite diameter of $Zn_3V_2O_8$ nanoparticles was about 40 nm.

3.2 FT-IR and EDX analysis

The surface conditioning of as-prepared $Zn_3V_2O_8$ nanoparticles was recorded using FT-IR spectrum in order to detect the residual organic compounds. Figure 2 shows FT-IR spectrum of sample No. 9. The absorption bond centered at 3431 cm^{-1} and weak peak at 1625 cm^{-1} can be assigned to the stretching and bending vibrations of the hydrogen-bonded OH groups of the adsorbed water, respectively. The vibration bonds at 843 and 668 cm^{-1} are attributed to tetrahedral VO_4 vibration modes in the network. The absorption around 419 cm^{-1} correspond to the streaching vibration Zn–O band, which is consistent with octahedral ZnO_6 [18, 19]. The vibration peaks at 1102 and 1222 cm^{-1} are assigned to S–O and absorption of CO_2 molecules from atmosphere, respectively [20, 21]. Very weak peaks around 2920 and 2850 cm^{-1} can be attributed to the asymmetric and symmetric stretching vibrations of aliphatic groups (–CH2–) n, respectively [22]. From the FT-IR result, it can be concluded that probably a small amount of SDS surfactant is attached to the surface of $Zn_3V_2O_8$ nanoparticles which may have a well role in preventing nanoparticles agglomeration.

EDX further confirmed that the nanoparticles are composed of $Zn_3V_2O_8$. The EDX of the sample No. 9 is shown in Fig. 3. Peaks associated with Zn, V and O are clearly observed and provide strong evidence that the nanocrystals are composed of only $Zn_3V_2O_8$.

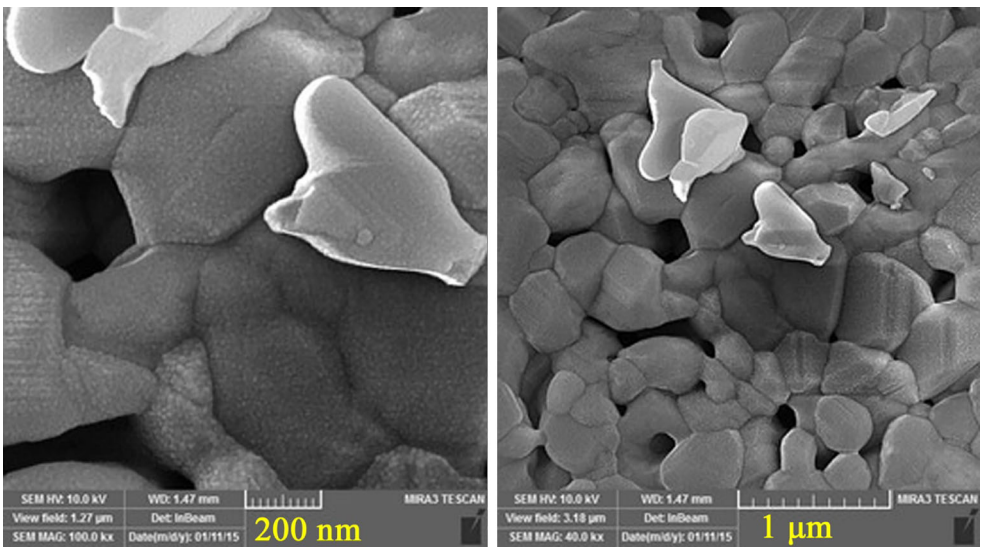

Fig. 5 SEM images of $Zn_3V_2O_8$ nanostructures prepared without amine (sample No. 7)

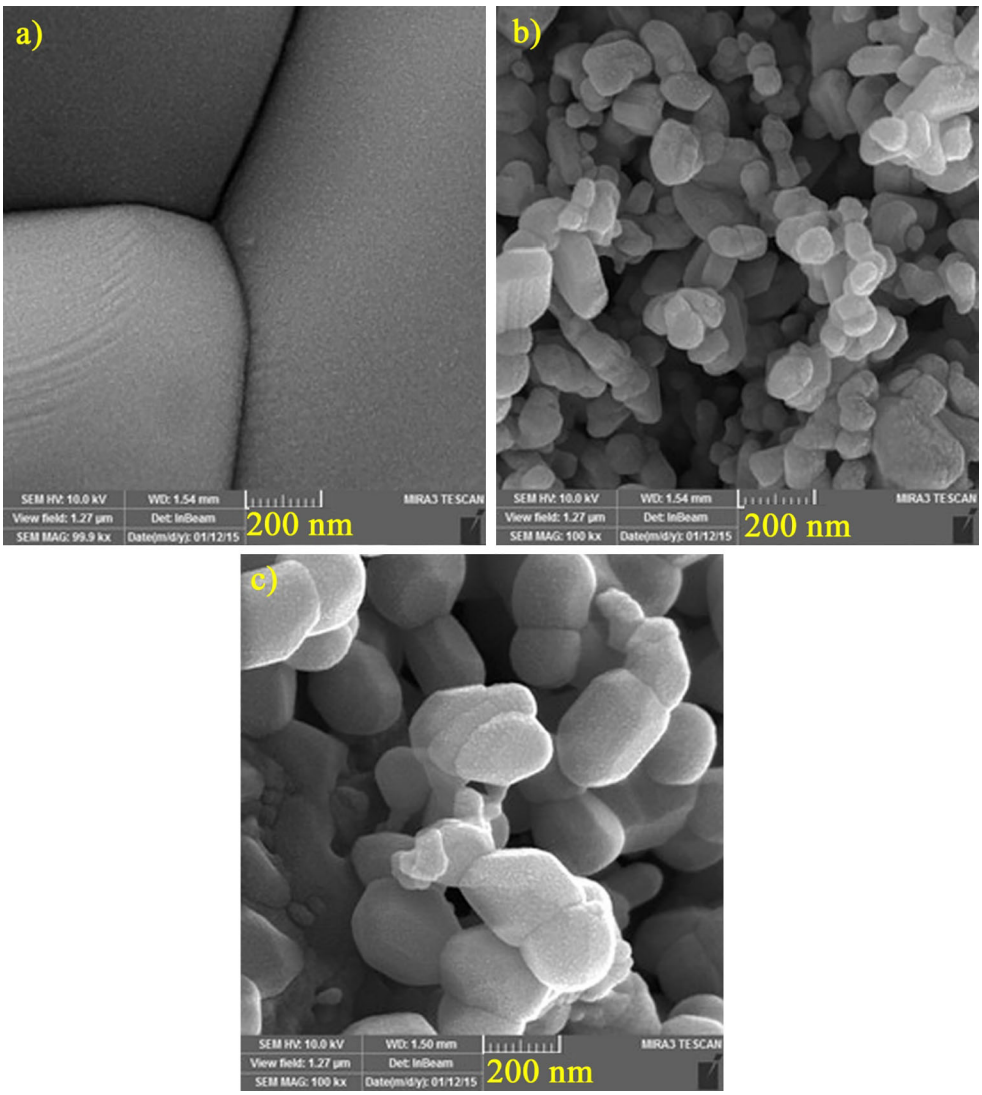

Fig. 6 SEM images of $Zn_3V_2O_8$ nanostructures prepared using of different surfactants **a** CTAB, **b** SDS and **c** PVP

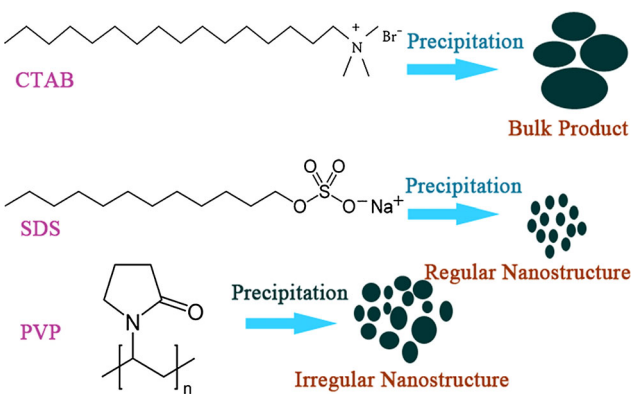

Scheme 2 Schematic diagram of formation of nanostructures and effect of CTAB, SDS and PVP on the size, morphology and uniformity of products

3.3 SEM and TEM images

The effect of different amines on surface morphologies and size of the obtained $Zn_3V_2O_8$ products is shown in Fig. 4. Figure 4a–f show prepared Zinc Vanadium Oxide nanostructures by NH_3, en, pn, bn, TETA and TEPA (sample No. 1–6), respectively. The used different amines for preparation of product are shown in Scheme 1. The average particle sizes of samples obtained from SEM images are listed in Table 1. As shown in Fig. 4a–d, the morphology of the samples $Zn_3V_2O_8$ synthesized by NH_3 as a monodentate amine and en, pn and bn as bidentate amines is spherical and ellipsoids nanoparticles. Although morphologies of the samples No. 1–4 are the same (spherical and ellipsoids nanoparticles), the size and uniformity of nanoparticles are

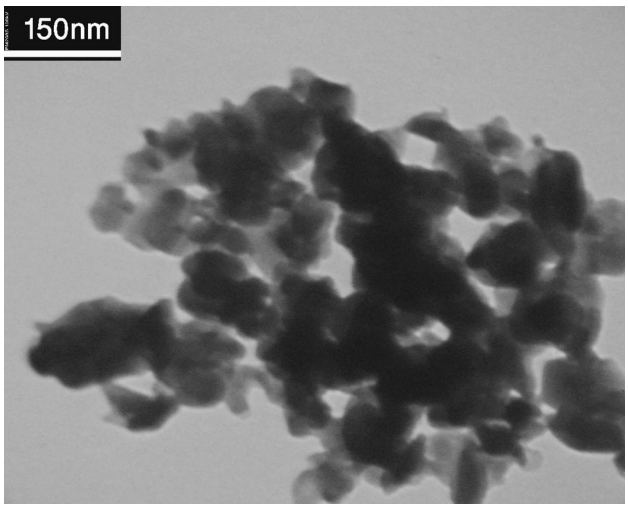

Fig. 7 TEM image of $Zn_3V_2O_8$ nanostructures by SDS surfactant (sample No. 9)

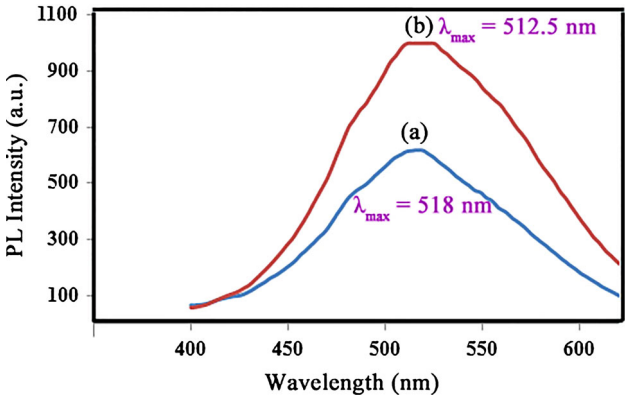

Fig. 9 Room temperature photoluminescence of *a* sample. No. 7 and *b* sample No. 9

different. The $Zn_3V_2O_8$ product synthesized by en amine is optimum product because nanoparticles have smaller size and more uniformity. In Fig. 4e, f, it can be seen that agglomerated nanoparticles of $Zn_3V_2O_8$ are formed with the aid of TETA and TEPA, respectively.

To study the effect of the amine on the size and morphology of the $Zn_3V_2O_8$ nanostructures, the experiment was carried out without using any amine (blank test). It is noted that other synthesizing conditions was unchanged in the blank test. The typical SEM image of the product obtained from the blank test is seen in Fig. 5. As shown in this image, the particles are highly agglomerated, and it is difficult to measure the individual particle size. Therefore, it was observed that the use of the amine as size controller

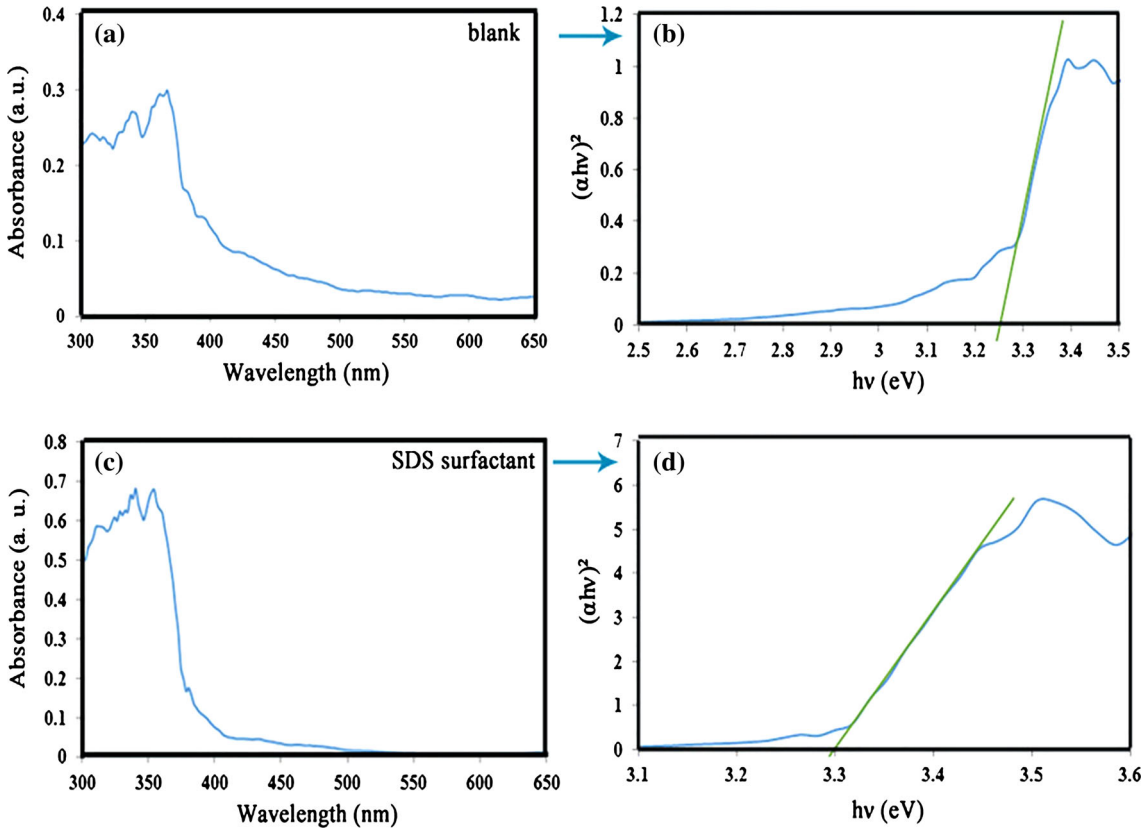

Fig. 8 **a**, **c** UV–Vis diffuse absorption spectra and **b**, **d** plot of $(\alpha h\nu)^2$ versus $(h\nu)$ of sample No. 7 and 9, respectively

is a key factor to the formation of dispersed $Zn_3V_2O_8$ nanoparticles. On the other hand, self-assembly of the $Zn_3V_2O_8$ nuclei prepared at the early stage of the reaction depends on the coordination mode of the amine.

SEM images of synthesized $Zn_3V_2O_8$ products using different surfactants with en amine selected as optimum amine are showed in Fig. 6. Figure 6a–c show SEM images of $Zn_3V_2O_8$ product with different surfactants such as anionic (SDS), cationic (CTAB) and polymeric (PVP) are illustrated in, respectively. These results show that using CTAB lead to synthesis of bulk products. By comparing SEM images of Fig. 6b, c, it can be seen that particle size of $Zn_3V_2O_8$ synthesized by SDS are smaller than those produced by PVP. Among these used surfactants, SDS generates the highest steric hindrance effect. The SDS plays capping agent role by hindering the aggregation of the nanoparticles. As illustrated in Fig. 6a–c, by increasing the steric hindrance influence, the size of the particles becomes small. It seems that when steric hindrance influence enhances, the nucleation to be occurred rather than the particle growth. Therefore, SDS surfactant is suitable for preparing of fine and uniform $Zn_3V_2O_8$ nanoparticles. Schematic diagram of formation of $Zn_3V_2O_8$ product by different surfactants is depicted in Scheme 2.

The size and morphology of the products were analyzed by the TEM image (Fig. 7). Figure 7 reveals that the $Zn_3V_2O_8$ nanoparticles (sample No. 9) prepared with SDS surfactant and precipitation method consisting sphere-like nanoparticles with average particle size of 25–110 nm.

3.4 Optical properties

The UV–Vis Diffuse Reflectance spectroscopy of sample No. 7 and 9 are shown in Fig. 8a–d. As shown in this figure the position of absorption edges are various. In comparison to the blank product (Fig. 8a) the absorption edge of SDS sample shift to blue region. This shift increases UV light absorption and hence is useful for photocatalysis application. The fundamental absorption edge in most semiconductors follows the exponential law. Using the absorption data, the band gap was estimated by Tauc's relationship:

$$\alpha = \frac{\alpha_0 \left(h\upsilon - E_g\right)^n}{h\upsilon}$$

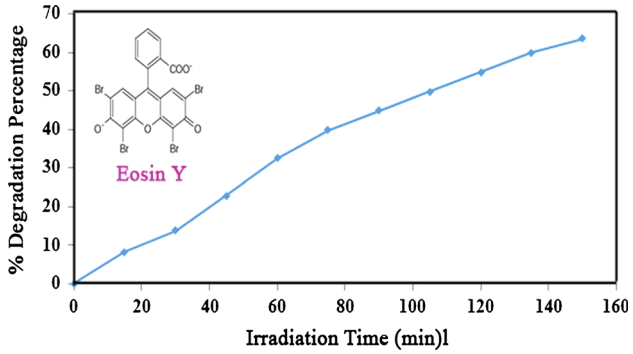

Fig. 10 Photocatalytic eosin Y degradation of $Zn_3V_2O_8$ nanoparticles under UV irradiations

Scheme 3 Schematic diagram of different electronic transitions for DRS and PL test

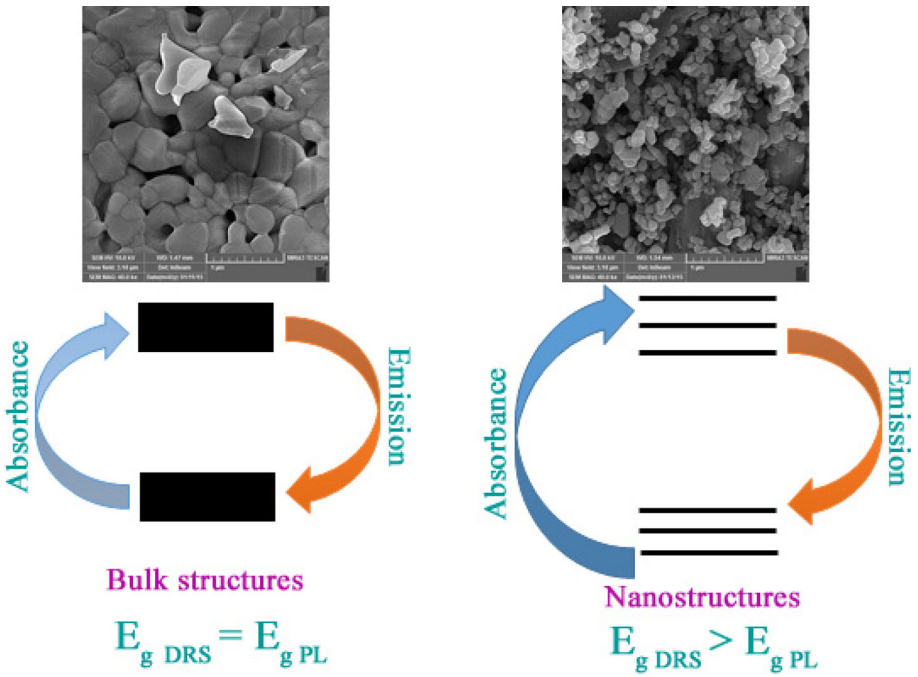

where α is absorption coefficient, hν is the photon energy, α_0 and h are the constants, E_g is the optical band gap of the material, and n depends on the type of electronic transition and can be any value between ½ and 3 [23]. The energy gaps of the samples have been determined by extrapolating the linear portion of the plots of $(\alpha h\nu)^2$ against hν to the energy axis (Fig. 8b, d). The E_g values are calculated 3.25 and 3.3 eV for the samples No. 7 and 9, respectively. By decreasing of particles size, energy gap increased. The difference of band gap values have been attributed to variations in the impurities content, the crystalline size and the type of electronic transition [24, 25]. Moreover, Optical properties of $Zn_3V_2O_8$ nanocrystals were investigated by using PL technique. Optical properties of zinc vanadate nanocrystals are of great importance as they provide information for the uses of these materials in photocatalytic applications. Figure 9a, b shows the PL spectrum of $Zn_3V_2O_8$ nanostructures of sample No. 7, 9 with different size and morphology that measured at room temperature using an excitation wavelength of 320 nm. A strong visible light emission ranging from 450 to 600 nm can be found in the PL spectrum. The PL spectra show a broad emission band centered at around 518 and 512.5 nm for sample No 7 and 9, respectively. The PL emission in $Zn_3V_2O_8$ nanostructures exhibits well dependence on particle size and morphology. As the crystallite size decreases, intensity of emission peaks increase and the peaks shift to higher frequencies, which is ascribed to the increase in the content of surface oxygen vacancy and defect with decreasing particle size. The high intensity of PL signal of sample No. 9 in Fig. 9b is attributed to its smaller particle size than the samples no. 7. The determined band gap of sample no. 7, 9 in ethanol solution are 2.39 and 2.41 eV, respectively [11, 18]. The calculated band gap from PL test is lower than DRS test. The type of transition electronic of absorbance and emission are shown in Scheme 3 for DRS and PL test, respectively.

3.5 Photocatalytic and magnetic properties

The photocatalytic activity of pure $Zn_3V_2O_8$ nanoparticles (sample No. 9) was investigated by monitoring the degradation of eosin Y as water pollutant in an aqueous solution under UV light irradiation. The obtained results are shown in Fig. 10. As shown in Fig. 10, the eosin Y degradation percentage of $Zn_3V_2O_8$ nanoparticles increased rapidly after the Osram lamp turned on. According to photocatalytic calculations by Eq. (1), the MO degradation was about 63.6 % after 150 min irradiation of UV light. These results indicated that pure $Zn_3V_2O_8$ nanocrystals are suitable photocatalyst under UV light in the short time. It is well known that the size, crystallinity, morphology and surface areas of nanostructures as photocatalyst have significant effect on the photocatalytic activity [26]. On the other hand, the defects in crystals, such as zinc vacancy, oxygen vacancy, especially on the surface can supply more active sites are considerable to photocatalyst during the catalytic process [27]. The heterogeneous photocatalytic processes involve many stages, such as diffusion, adsorption and reaction, appropriate distribution of the pore is usefull to diffusion of reactants and products, which favors the photocatalytic reaction. In this work, the modified photocatalytic activity may be attributed to convenient distribution of the pore, numerous hydroxyl content and high separation rate of photoinduced charge carriers [28–34]. Moreover, magnetic properties of $Zn_3V_2O_8$ nanostructures prepared in presence of SDS surfactant were investigated. Figure 11 exhibits the magnetic properties of

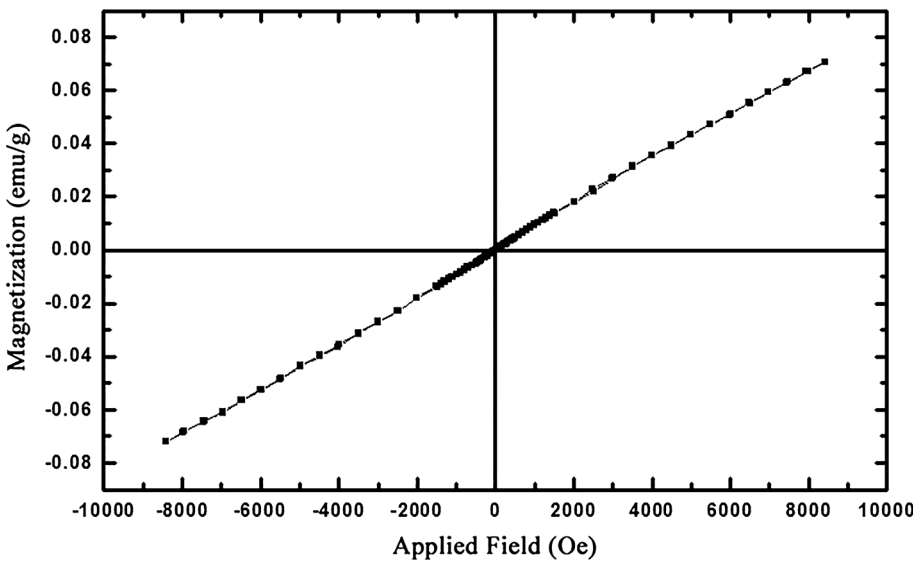

Fig. 11 Magnetization versus applied magnetic field at room temperature for the $Zn_3V_2O_8$ nanostructures (sample No. 9)

the as-prepared sample No. 9 with uniform nanoparticles. As seen in Fig. 11, sample no. 9 presents paramagnetic behavior.

4 Conclusions

We employed a facile precipitation method to synthesize pure $Zn_3V_2O_8$ nanoparticles with aid of different amines as basic agent and size controller. CTAB, SDS and PVP were used as the capping agents. $Zn_3V_2O_8$ nanocrystals were characterized by XRD, SEM, TEM, EDS, FT-IR, PL and DRS. Different morphology and size of products were prepared. Optimum amine and surfactant for fine and uniform nanoparticles synthesis were selected. The photocatalytic behavior of nanoparticles was evaluated using the degradation of eosin Y aqueous solution under UV light irradiation. The results show that $Zn_3V_2O_8$ nanostructures are good candidate with excellent performance in photocatalytic applications for degradation of anionic dye under UV irradiation in a short time.

Acknowledgments Authors are grateful to the council of Iran National Science Foundation and University of Kashan for supporting this work by Grant No (159271/342).

References

1. R. Costi, A.E. Saunders, U. Banin, Angew. Chem. Int. Ed. **49**, 4878 (2010)
2. R. Kubo, A. Kawabata, S. Kobayashi, Annu. Rev. Mater. Sci. **14**, 49 (1984)
3. A.M. Smith, S. Nie, Acc. Chem. Res. **43**, 190 (2010)
4. M. Masato, M. Yui, M. Yuichi, I. Keita, Chem. Commun. **47**, 9591 (2011)
5. L.Q. Mai, L. Xu, C.H. Han, X. Xu, Y.Z. Luo, S.Y. Zhao, Y.L. Zhao, Nano Lett. **10**, 4750 (2010)
6. A.M. Crespi, S.K. Somdahl, C.L. Schmidt, P.M. Skarstad, J. Power Sources **96**, 33 (2001)
7. G. Liu, J.E. Greedan, J. Solid State Chem. **114**, 499 (1995)
8. L.H. Gan, D. Deng, Y. Zhang, G. Li, X. Wang, L. Jiangb, C.R. Wang, J. Mater. Chem. A. **2**, 2461 (2014)
9. C. Mondal, M. Ganguly, A.K. Sinha, J. Pal, R. Sahoo, T. Pal, Cryst Eng Comm. **15**, 6745 (2013)
10. S. Shreyas, Mukut Pitale, I.M. Gohain, O.M.Ntwaeaborwa Nagpure, Barend C.B. Bezuidenhoudt, H.C. Swart, Phys. B. **407**, 1485 (2012)
11. T. Li, J. Luo, Z. Honda, T. Fukuda, N. Kamata, Adv. Mater. Phys. Chem. **2**, 173 (2012)
12. R. Shi, Y. Wang, F. Zhou, Y. Zhu, J. Mater. Chem. **21**, 6313 (2011)
13. L. Xiao, Y. Zhao, J. Yin, L. Zhang, Chem. Eur. J. **15**, 9442 (2009)
14. D. Wang, J. Tang, Z. Zou, J. Ye, Chem. Mater. **17**, 5177 (2005)
15. M. Salavati-Niasari, N. Mir, F. Davar, J. Alloys Compd. **493**, 163 (2010)
16. M. Salavati-Niasari, N. Mir, F. Davar, Polyhedron **28**, 1111 (2009)
17. H.P. Klug, L.F. Alexander, *X-ray Diffraction Procedures for Polycrystalline and Amorphous Materials*, 2nd edn. (John Wiley and Sons Press, 1954)
18. S. Ni, X. Wang, G. Zhou, F. Yang, J. Wang, D. He, J. Alloys Compd. **491**, 378 (2010)
19. M. Wang, Y. Shi, G. Jiang, Mater. Res. Bull. **47**, 18 (2012)
20. L. Salavati-Niasari, F.M. Saleh, A. Ghaemi, Ultrason. Sonochem. **21**, 653 (2014)
21. H. Dong, Z. Du, Y. Zhao, D. Zhou, Powder Technol. **198**, 325 (2010)
22. Y. Liu, D. Wang, J. Sun, Renew. Energy. **38**, 214 (2012)
23. J. Tauc, R. Grigorovici, A. Vancu, J. Phys. Status Solidi B. **15**, 627 (1966)
24. M. Hidalgo, M. Aguilar, M. Maicu, J. Navio, G. Colon, J. Catal. Today **129**, 50 (2007)
25. F. Hossain, L. Sheppard, J. Nowotny, G. Murch, J. Phys. Chem. Solids **69**, 1820 (2008)
26. H. Huang, H.F. Chen, Y. Xia, X.Y. Tao, Y.P. Gan, X.X. Weng, W. Zhang, J. Colloid Interface Sci. **370**, 132 (2012)
27. X.J. Wang, Q.L. Zhang, Q. Wan, G.Z. Dai, C.J. Zhou, B.S. Zou, J. Phys. Chem. C **115**, 2769 (2011)
28. J. Zhong, J. Li, F. Feng, Y. Lu, J. Zeng, W. Hu, Z. Tang, J. Mol. Catal. A: Chem. **357**, 101 (2012)
29. D. Ghanbari, M. Salavati-Niasari, S. Karimzadeh, S. Gholamrezaei, J. Nanostruct. **4**, 227 (2014)
30. G. Nabiyouni, S. Sharifi, D. Ghanbari, M. Salavati-Niasari, J. Nanostruct. **4**, 317 (2014)
31. M. Panahi-Kalamuei, M. Mousavi-Kamazani, M. Salavati-Niasari, J. Nanostruct. **4**, 459 (2014)
32. F. Beshkar, M. Salavati-Niasari, J. Nanostruct. **5**, 17 (2015)
33. M. Goudarzi, D. Ghanbari, M. Salavati-Niasari, J. Nanostruct. **5**, 110 (2015)
34. S. Moshtaghi, M. Salavati-Niasari, D. Ghanbari, Summer J Nanostruct. **5**, 169 (2015)